Titanium dioxide/silver nanoparticle bilayers prepared in self-assembly processes

Julia Maciejewska[*], Magdalena Oćwieja, Zbigniew Adamczyk,
Elżbieta Bielańska and Bogna Napruszewska

Jerzy Haber Institute of Cataysis and Surface Chemistry
Polish Academy of Sciences
Niezapominajek 8,30-239 Cracow, Poland
[*]*e-mail: ncmaciej@cyf-kr.edu.pl*

A method for the preparation of TiO_2/Ag bilayers via colloid self-assembly process using well-characterized titanium dioxide and silver suspensions was developed. The titanium dioxide nanoparticles, forming a supporting layer, were 46 nm in diameter, exhibiting an isoelectric point at pH 6.4. The silver nanoparticles, forming an external layer of the diameter of 50 nm were prepared via a chemical reduction method with the presence inorganic phosphate salts. The electrophoretic mobility measurements revealed that the zeta potential of silver nanoparticles was highly negative for a broad range of pH and ionic strengths. By explaining this information, the optimum condition for the silver nanoparticle immobilization on TiO_2 supporting layers were selected. The coverage of the first layer was adjusted by ionic strength of the suspensions and by the deposition time. Afterward, the silver nanoparticle monolayers of controlled coverage were deposited under the diffusion-controlled transport. Their coverage was determined by a direct enumeration of deposited nanoparticles from AFM images and SEM micrographs. The experimental results showed that for extended deposition times, the coverage of silver nanoparticle layers significantly increases with ionic strength. Therefore, it was proven that the formation of bilayers is mainly controlled by electrostatic interactions and that it is feasible to produce uniform TiO_2/Ag materials of desired coverage and structure.

1. INTRODUCTION

Titanium dioxide nanoparticles are widely applied in various branches of science and industry. Thanks to high chemical and physical stability and unique properties, they are used in various areas of photocatalysis [1,2], photoelectronics [3,4] and optics [5]. Furthermore, titanium dioxide is an efficient and inexpensive photocatalyst due to strong oxidation capacity, favorable opto-electronic properties and biocompatibility [1,6]. The advantages of titanium dioxide nanoparticles are: a strong resistance to chemicals and photocorrosion, a low operation temperature and a significantly low energy consumption [7].

In recent years, it was also revealed that the photoelectrochemical properties of titanium dioxide nanoparticles can be efficiently tuned using silver, gold, platinum and palladium nanoparticles [7,8]. The doping and coating of titanium dioxide nanoparticles and films with transition or noble metal causes an enhancement of quantum yield [9], an activation of wide bandgap toward visible light [10] and an increase in the rate of the photocatalytic reactions [11].

The usual methods of titanium dioxide modification by noble metals are thermal impregnation [12], chemical vapour deposition (CVD) [13], photodeposition [14,15] and sol-gel preparation [16]. However, it was reported [1] that these 'dry' chemical and ceramics methods, where heating or annealing at high temperatures are important steps in the preparation process, are too complicated for large-scale production.

In the case of photodeposition, the first step of monolayer preparation consists in the impregnation on titanium dioxide by metal ions and then the photoreduction, which leads to formation of nanoparticles. This method of titanium dioxide doping is often used for practical applications, despite of the fact that it exhibits some disadvantages. It is worth pointing out that in many cases the monolayers obtained in the photoreduction processes are characterized by a heterogeneous distribution of metal nanoparticles within the titanium dioxide surfaces. On the other hand, the amount of metals depends on various parameters such as the precursor ion concentration, the wavelength and intensity of the light and the time of the exposure [1, 4]. Moreover, several studies showed that despite of the strict control of the governing parameters of photoreduction, the process is not reproducible. Therefore, tuning of plasmonic and photocatalytic properties of titanium dioxide materials doped with metal nanoparticles still remains a challenge.

Taking into account that the most titanium dioxide modifications are conducted using silver, in this work, we proposed the preparation of well-defined TiO_2/Ag bilayers by exploiting colloid self-assembly process using well-characterized titanium dioxide and silver suspensions. The kinetics of silver nanoparticle deposition on titanium dioxide monolayers was studied by atomic force microscopy (AFM) and scanning electron microscopy (SEM). The processes were carried out under diffusion-controlled conditions at selected pH and ionic strength conditions which allows to determine the influence of these parameters on the formation of TiO_2/Ag bilayers.

2. MATERIALS AND METHODS

2.1. Synthesis of silver nanoparticles

All chemicals were used as received without a further purification. Silver nitrate, sodium hydroxide, sodium hypophosphite, sodium hexametaphosphate and titanium dioxide suspension (33-37 wt. % in H_2O, 700346-25G) were purchased from Sigma Aldrich (Poznan, Poland). Hydrochloric acid and sodium hydroxide were supplied by Avantor Performance Materials Poland S.A. (formerly POCH S.A., Gliwice, Poland). Ultrapure water, used throughout the studies, was obtained using Milli-Q Elix & Simplicity 185 purification system from Millipore S.A. (Molsheim, France). Naturaly ruby mica sheets, supplied by Continental Trade (Warszawa, Poland), was used as a substrate for the deposition of colloid particles.

The silver nanoparticles used during the studies, were prepared by chemical reduction of silver ions using inorganic phosphate salts. In contrast to well-known methods of silver preparation under basic conditions [19, 20], this synthesis was carried out under acidic conditions. As it was shown in the work of Liu and Yu [21], at pH 2.0–2.9 an inactive hypophosphite anion, is convert reversibly to a metastable form containing two hydroxyl groups. This tautomer of hypophosphite is involved in the reduction of silver ions. Since, the oxidized form of hypophosphite is a poor stabilizing agent, in classical method the synthesis of silver nanoparticles is conducted in the presence of surfactants or polymers [21]. In our modification, these high molecular weight compounds were replaced by sodium hexametaphosphate which exhibits an excellent stabilizing properties that allows to obtain silver suspensions of high antibacterial properties [22, 23]. After the synthesis,

the suspension was cooled to a room temperature and purified from ionic excess using a filtration cell (Millipore, model 8400) equipped with a polyethersulfone ultrafiltration discs (Millipore, 100 kDa, PBHK07610 model). The ultrafiltration was carried out until the conductivity of suspension attained a minimum value of 15–20 μS/cm and pH 5.5–6.0. The effluent also was used in the next stages of studies.

2.2. Methods

The weight concentration of silver particles in the suspensions was precisely determined using the densitometer. It was found that the concentration of stock silver solution was 256 mg/dm^3. On the other hand, the concentration of TiO$_2$ suspension was determined by the gravimetric measurements. Three samples of TiO$_2$ suspension of known volume were dried at a temperature of 120°C until the mass of the powder attained a constant value. It was calculated that the concentration of stock solution was equal to 31 g/dm^3.

In order to obtain TiO$_2$/Ag particle bilayers, in the first step, freshly cleaved mica sheets were immersed in a thermostated diffusion cell containing titanium dioxide suspensions of of bulk concentration equal to 1000 mg/dm^3, $I = 0.01$ M NaCl, pH 4.0 and kept over the time of 2 hours. The diffusion cell was a cylindrical glass vessel with a capacity of 6 ml placed in thermostated chamber. The cell was equipped with a glass elements, which allow to maintain the mica sheets in a vertical position. Therefore, the deposition of particles occurred under purely diffusion-controlled transport. After the proper deposition time, the mica sheets with TiO$_2$ monolayers were removed from the suspensions, rinsed with ultrapure water and placed in a thermostated diffusion cell containing the silver suspensions of a desired concentration (5–100 mg/dm^3), ionic strength (0.1 mM–30 mM NaCl) and pH (3.0–10.0). The deposition time for silver suspensions varied between 5 and 900 minutes in order to obtain bilayers of controlled coverage of metallic particles. Finally, the TiO$_2$/Ag particle bilayers were removed from suspensions, cleaned in ultrapure water, in order to remove the unbounded particles and the excess of sodium chloride, and air dried. Finally, the samples were characterized using the techniques described below.

The conductivity and pH of the suspensions were measured using the multifunctional device CPC-505 supplied by Elmetron company. The density of suspensions and their effluents, obtained during the ultra-filtration, were measured using Anton Paar densitometer (DMA5000 M). Knowing these parameters well as the specific density of silver and

titanium dioxide, the weight fraction of particles in the suspensions was calculated using the approach described in our previous works [17, 18].

UV-vis spectra of suspensions were recorded with a 1 cm path length quartz cell using the Shimadzu UV-1800 spectrometer. Ultrapure water was used as the reference sample to take the 'blank' spectrum for all measurements.

The crystal structure and purity of the dried particle powders were confirmed by X-ray diffraction analysis. The diffractograms were recorded using the PAN analytical X' PERT PRO (Cu Ka, 40 kV, 30 mA) instrument.

Particle size in the suspensions, polydispersity index and stability under various pHs and ionic strengths were determined from the dynamic light scattering (DLS) measurements using ZetaSizer Nano ZS apparatus from the Malvern company. On the other hand, the electrophoretic mobility measurements of particles, conducted using ZetaSizer Nano ZS, allow to determine their zeta potentials.

The surface concentration of titanium dioxide particles, forming the first layer, was quantitatively determined using the atomic force microscopy (AFM) working in semi-contact mode using silicon probe (polysilicon cantilevers with resonance 120 kHz, typical curvature radius tip was 10 nm, cont angel was $< 20°$). The imaging was done using the NT-MDT Solver Pro instrument with the SMENA SFC050L scanning head.

The scanning electron microscope JEOL JSM-7500F was used to determine the morphology of silver and titanium dioxide particles (transmission mode) and the coverage of TiO_2/Ag nanoparticle bilayers. The coverage of bilayers was investigated with the application of a backscattered electron (BSE) detector that makes it possible to contrast and separate the investigated material in COMPO mode. In this kind of measurements, the samples were covered with a thin layer of chromium before the investigation to ensure a sufficient conductivity. The number of particles per unit area of the substrate was determined from these AFM images or SEM micrographs using image-analysis software MultiScan Base. Typically, the number of particles was determined over 10–15 equally sized areas randomly chosen over the TiO_2-precovered mica sheet.

3. RESULTS AND DISCUSSION

3.1. X- ray diffraction measurements

The crystal structure and purity of dried silver and titanium dioxide samples were determined with the use of X-ray diffraction measurments. The obtained XRD patterns are presented in Fig. 1.
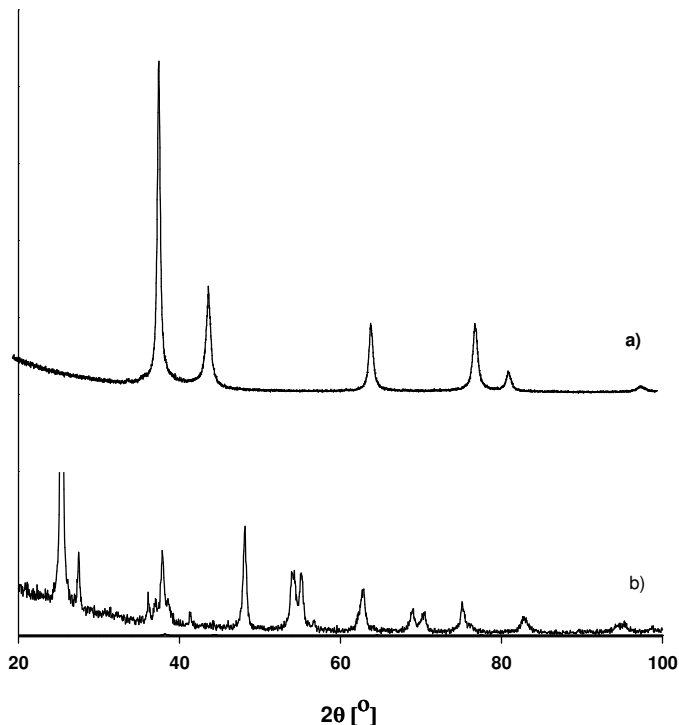

Fig. 1. Diffraction patterns recorded for: a) silver and b) titanium dioxide particles.

In the case of silver particles (Fig. 1a), one can observe five strong Bragg reflections appearing at 38.1°, 44.1°, 64.5°, 74.3° and 81°. They are pertaining to (111), (200), (220), (311) and (222) planes of a face centered cubic (fcc) lattice of silver. The diffraction patter of dried sample of titanium dioxide exhibit more diffraction peaks. One can observe Bragg reflections appeared at 27.5°, 37.0°, 37.8°, 41.3° which correspond to (110), (101), (200) and (111) planes of a tetragonal (P42/mnm) lattice of ruthyl (PDF#04-004-4337). On the other hand, the diffraction peaks at 25.3°, 48.1°, 53.9°, 55.1°, 62.8°, 69.0°, 75.2° correspond to (101), (200), (105), (211), (204), (116) and (215) place of a tetragonal (I41/amd) lattice

of anathase (PDF#04-016-2837). The phase content of the samples was determined from the integrated intensities of anatase (101) and rutile (110) peaks accoriding to the formulas described elsewhere [24]. It was found that the phase content of anathase was 85% and 15% in the case of ruthyl.

3.2. UV-Vis spectroscopy

In the next series of experiments, spectrophotometer was used in order to characterize the absorption properties of suspensions. The stock solutions of both samples were diluted to 20-25 mg/dm^3 and the UV-vis spectra of these suspensions were recorded. As can be seen (Fig. 2), the silver suspension exhibits a characteristic absorption maximum at the wavelength of 405 nm. The band is narrow and symmetric which suggests that the particles are spherical and rather monodisperse [25]. In the case of titanium dioxide suspension, one can observe a wide absorption band in the UV region at the wavelength 200-300 nm. This is consistent with the results described in the literature for titanium dioxide suspensions free from impurities [26].
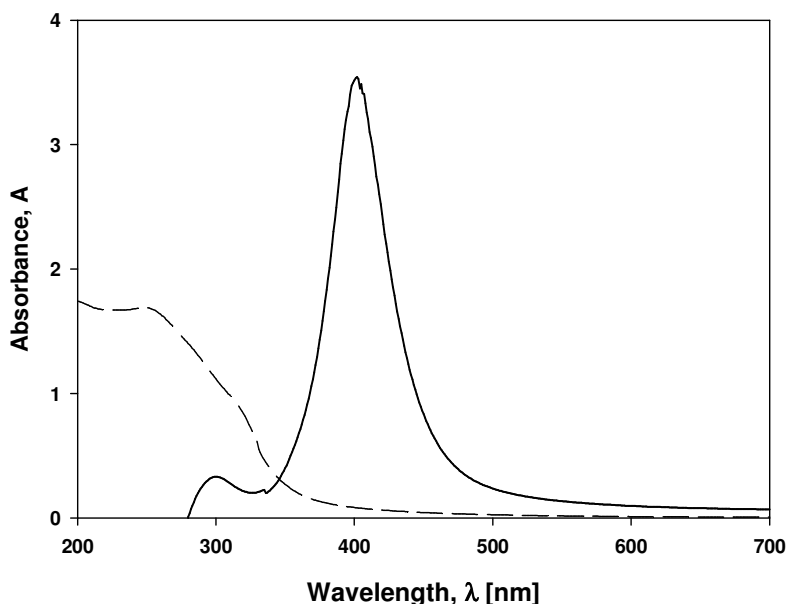

Fig. 2. UV-vis spectra of: (−) silver and (– – –) titanium dioxide suspensions. The concentration of particles in the solutions 20–25 mg/dm^3.

3.3. Dynamic Light Scattering results

The stability of nanoparticles under controlled conditions of ionic strength and pH were studied using the dynamic light scattering technique (DLS). The diffusion coefficients measured by DLS are used to calculate the hydrodynamic diameters of particles using the Stokes-Einstein relationship [22, 23]. The stock solutions of both types of nanoparticles were diluted to the concentration of 200 mg/dm^3. Afterward, pH and the electric conductivity of these solutions were measured. It was revealed that pH of titanium dioxide suspension attained 4 and the silver suspension exhibited pH of 5.5. The electric conductivity of both solutions remained at constant value of 10 µS/cm.

The ionic strength of suspensions was regulated by the addition of sodium chloride. The dependence of hydrodynamic diameter of nanoparticles on ionic strength, for above mentioned values of pH, is shown in Fig. 3.
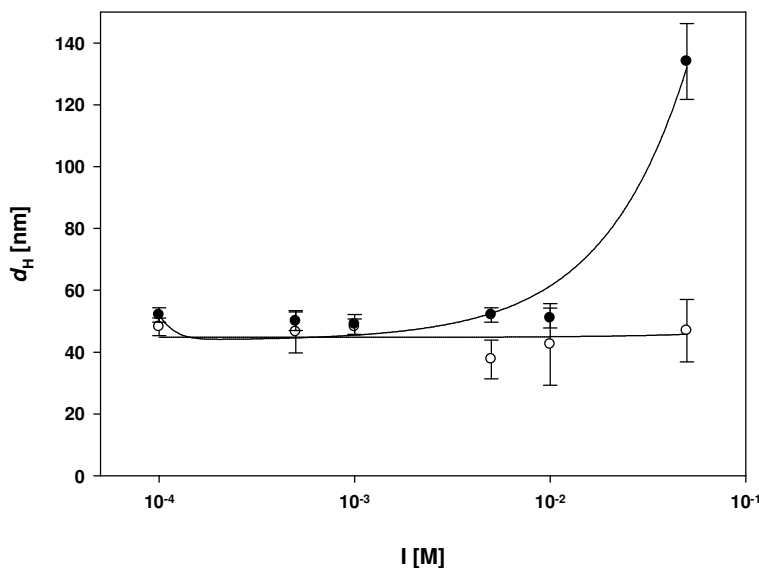

Fig. 3. The dependence of hydrodynamic diameter of (○) titanium dioxide and (●) silver nanoparticles on ionic strength determined for suspension concentration of 200 mg/dm^3 and pH (○) 4.0 and (●) 5.5.

As can be noticed, the hydrodynamic diameter of titanium dioxide nanoparticles attains a constant value of 46 nm, within error boundaries, ± 5 nm of ionic strength. On the other hand, the size of silver nanoparticles remains unchanged for ionic strength below 0.01 M NaCl and is equal to 50 ± 4 nm. For higher values, one can notice

a significant increase in the hydrodynamic diameter which suggests the aggregation of nanoparticles.

In the next stage of experiments, the dependence of hydrodynamic diameter on pH for constant ionic strength of 0.01 M NaCl was determined. The results of investigations are shown in Fig. 4. As can be noticed, for the pH 2.2-4.8, the hydrodynamic diameter of titanium dioxide nanoparticles remains constant. A considerable increase in the hydrodynamic diameter is observed for pH range 5.1-9.0 suggesting that for these conditions, the suspension becomes unstable. On the other hand, for pH $\geq$ 9.0, the hydrodynamic diameter of titanium dioxide nanoparticles again attains a stable value of 48 nm. In the case of the silver suspension, one can notice that nanoparticles aggregate at pH > 8.0. Below this value, the hydrodynamic diameter of nanoparticles equals to 50 nm.
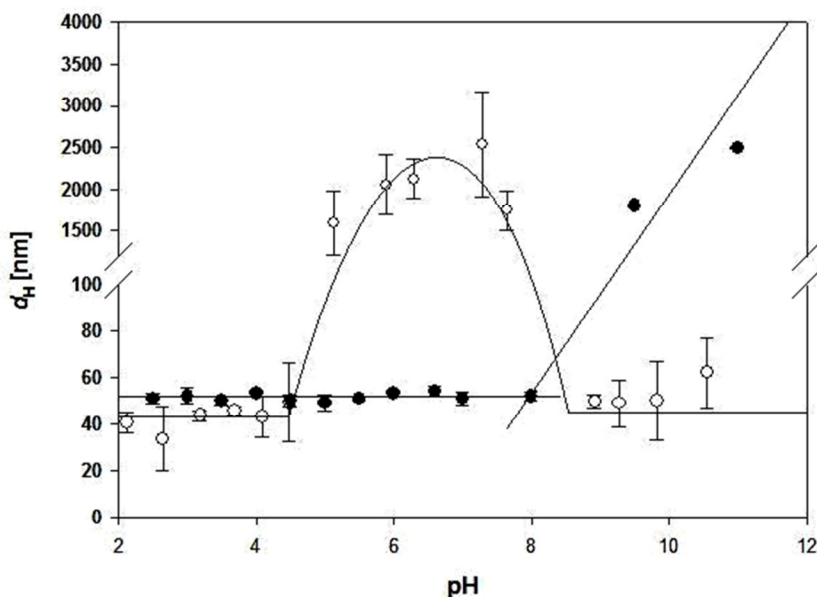

Fig. 4. The dependence of hydrodynamic diameter of ($\circ$) titanium dioxide and ($\bullet$) silver nanoparticles on pH for suspension concentration of 200 mg/dm^3 and ionic strength 0.01 M NaCl.

3.4. Microelectrophoresis results

Additionally, the measurements of the electrophoretic mobility (μ_e) of nanoparticles for controlled ionic strength and pH conditions were

carried out. By using the electrophoretic mobility data the zeta potential of nanoparticles was calculated using the Henry's equation:

$$\xi = \frac{3\eta}{2\varepsilon f(\kappa a_p)}\mu_e$$

where ξ is the zeta potential of nanoparticles, ε is the dielectric permittivity of water, μ_e the electrophoretic mobility, $f(\kappa a_p)$ is the function of the dimensionless parameter κa_p, where $\kappa^{-1} = \left(\frac{\varepsilon kT}{2e^2 I}\right)^{1/2}$ is the thickness of the electric double-layer, e is the elementary charge, $I = \frac{1}{2}\Sigma_i c_i z_i^2$ is the ionic strength, c_i the ion concentration, and a_p is the particle radius [22,23]. The dependence of zeta potential of nanoparticles on ionic strength is shown in Fig. 5, and the dependence of zeta potential on pH at ionic strength of 0.01 M NaCl is presented in Fig. 6.
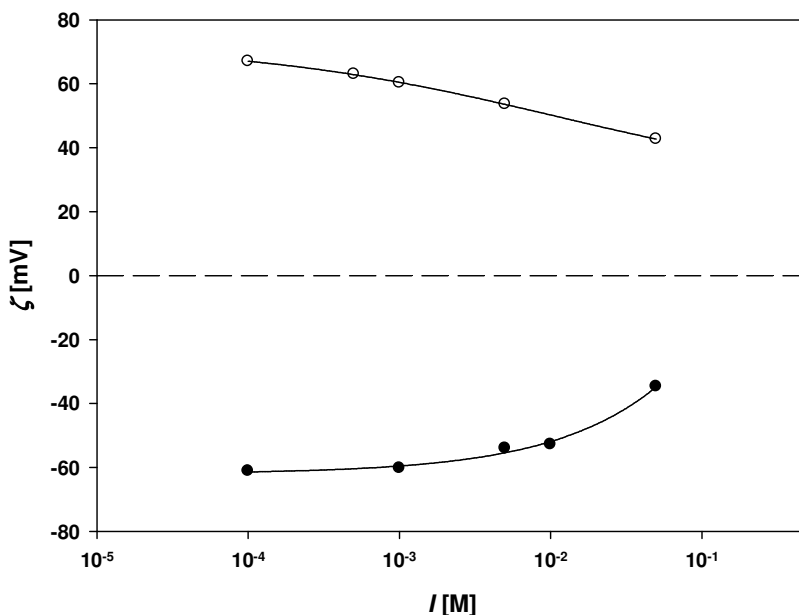

Fig. 5. The dependence of zeta potential of (○) titanium dioxide and (●) silver nanoparticles on ionic strength determined for suspension concentration of 200 mg/dm^3 and pH (○) 4.0 and (●) 5.5.

As can be noticed, the zeta potential silver nanoparticles is negative for the entire range of ionic strength (Fig. 5) and pH (Fig. 6), which indicates that the nanoparticles acquired a net negative surface charge.
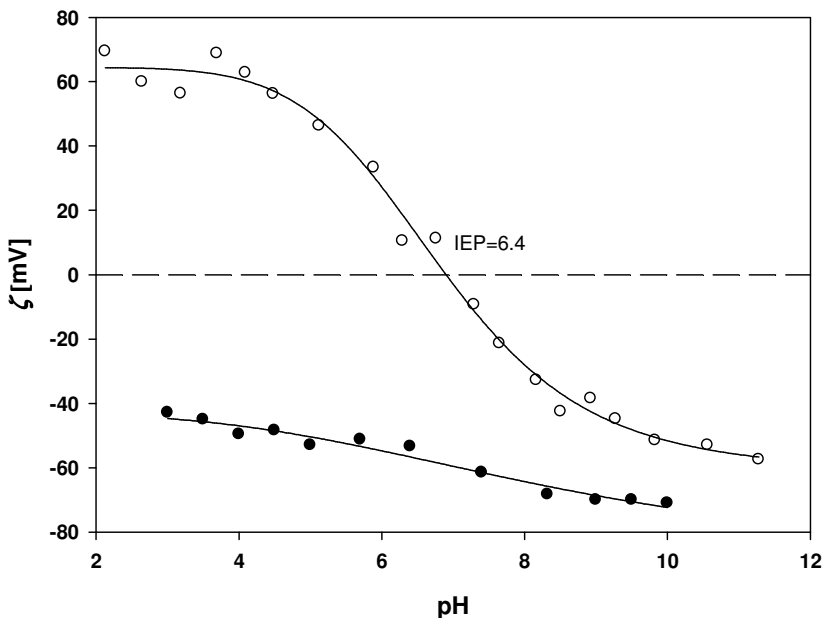
Fig. 6. The dependence of zeta potential of (○) titanium dioxide and (●) silver nanoparticles on pH for suspension concentration of 200 mg/dm^3 and ionic strength 0.01 M NaCl.

Moreover, one can observe a slightly increase in the zeta potential of silver nanoparticles with the ionic strong from –61 mV for 10^{-4} M NaCl to –34 mV for $3 \cdot 10^{-2}$ M NaCl. With the increase of pH, the zeta potential attains more negative values and equals to –43 mV at pH 3.0 and –54 mV at pH 9.0. In the case of the titanium dioxide, the zeta potential decreases with ionic strength from 67 mV for 10^{-4} M NaCl to 43 mV for $5 \cdot 10^{-2}$ M NaCl. Nonetheless, at pH 4.2 the nanoparticles are positively-charged for the entire range of ionic strength. As can be noticed in Fig. 6, the zeta potential of titanium dioxide nanoparticles strongly depends on pH. One can observe that the zeta potential of nanoparticles is positive for pH < 6.4 and negative otherwise. At pH 6.4, the titanium dioxide nanoparticles exhibit the isoelectric point. It is worth mentioning that the isoelectric point determined in our studies is in agreement with the results previously reported in the literature [27].

Taking into account that titanium dioxide nanoparticles exhibit a high positive surface charge and are stable at pH < 4.8, mica can be used as a model solid surface for their deposition because it is negatively charged at this pH. As it is known, mica is a chemical stable and molecular smooth material characterized by a uniform and homogenous

surface charge distribution [28, 29]. Moreover its surface potential is negative for a broad range of pH and ionic strengths [28]. Thus, the zeta potential of mica at pH 4.0 and ionic strength 0.01 M equals to –40 mV [29]. Based on this information, one can expect that an efficient deposition of titanium dioxide nanoparticles should take place on the mica surfaces.

3.5. Preparation and characteristic of titanium dioxide/silver nanoparticle bilayers

The homogenous titanium dioxide monolayers were produced as described in experimental part. Afterwards, the monolayers were imaged and characterized using microscopic techniques. The typical SEM images of titanium dioxide monolayers recorded in the secondary electron (a) and back scattered electron (b) modes are shown in Fig. 7.

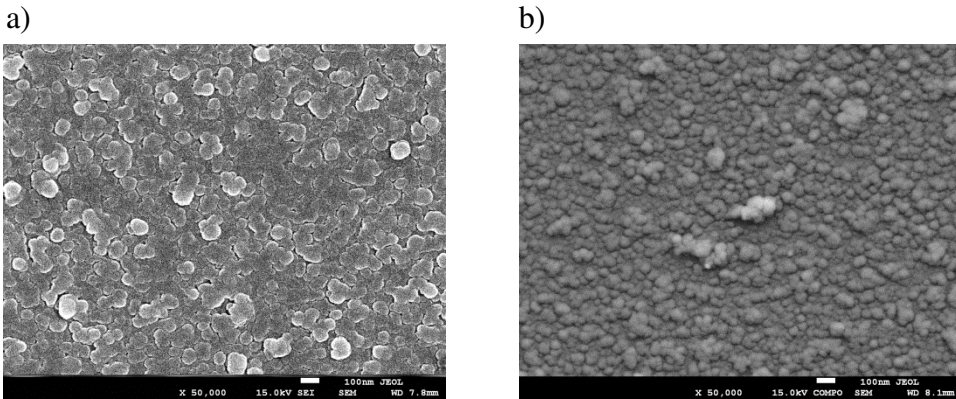a)   b)

Fig. 7. The image of titanium dioxide monolayer recorded in a) secondary electron mode and b) backscattered electron mode.

The surface concentration of particles was determined by a direct enumeration carried out using AFM and SEM imaging. The number of particles deposited on 8–10 equal-sized surface areas (typically having the dimensions of 2µm × 2µm) was determined. It was found that under these conditions, the surface concentration of titanium dioxide nanoparticles attained 325 μm^{-2}. Knowing the size of nanoparticles, one can express the surface concentration as a dimensionless coverage (θ) using simple equation: $\theta = \pi d^2 N_s/4$, where d is the diameter of titanium dioxide nanoparticles determined from DLS or TEM analysis and N_s is the nanoparticle surface concentration. Taking $d = 46$ nm, as determined above, it can be calculated that the coverage of titanium dioxide

nanoparticles is equal to 0.40. The deposition of titanium dioxide nanoparticles carried out for longer deposition times did not show any increase in the monolayer coverage. Hence, one can conclude that the used deposition conditions allowed to obtain homogeneous titanium dioxide monolayers of the highest coverage.

In the next step of our studies, the titanium dioxide monolayers were used as a platform for silver nanoparticle deposition. Considering that the zeta potential of titanium dioxide monolayers is positive in the same pH range as the nanoparticles in the bulk, and that the silver suspension is unstable for pH < 3.0, the formation of bilayers was investigated at pH 4.0 and for three ionic strengths of 10^{-4} M, 10^{-3} M and 10^{-2} M. The deposition experiments were conducted under diffusion-controlled transport according to the procedure described above. After a given deposition time, the dried bilayers were characterized using SEM. In order to perform quantitative studies on deposition kinetic of silver nanoparticles on titanium dioxide monolayers the measurements were conducted using SEM imaging with BSE detector working in the COMPO mode (Fig. 8). On the other hand, the energy dispersive spectroscopy (EDS) was applied in order to distinguish the both types of nanoparticles. As it was presented in the first spectrum, the external monolayer consists of silver nanoparticles whereas the bottom layer (second spectrum) is built up with the titanium dioxide nanoparticles. It is worth mentioning that the additional components come from mica surface, such as aluminum and silicon are also present in the spectra.

The kinetics of silver nanoparticle deposition on the titanium dioxide monolayers, shown as the dependence of nanoparticle surface concentration on the square root of deposition time, is presented in Fig. 9. As can be noticed, the surface concentration of silver nanoparticles linearly increases with the square root of time and is independent of ionic strength at shorter times. On the other hand, the maximum coverage increases with ionic strength. For the lowest ionic strength, the maximum surface concentration was attained after 9 minutes and equals to 20 μ/m^2. Taking into account that the size of the silver nanoparticles was 50 nm, one can calculate that the silver nanoparticle coverage is equal to 0.04. In the case of ionic strength 10^{-3} M, the linear increase of nanoparticle surface concentration with the square root of deposition time occurs for $t < 50$ min. After this period of time, the maximum surface concentration is attained which equals to 52 μm^{-2} ($\theta = 0.10$). The most dense silver nanoparticle monolayers, with the surface concentration of 122 μm^{-2} ($\theta = 0.23$), were obtained at the highest ionic strength of 10^{-2} M.

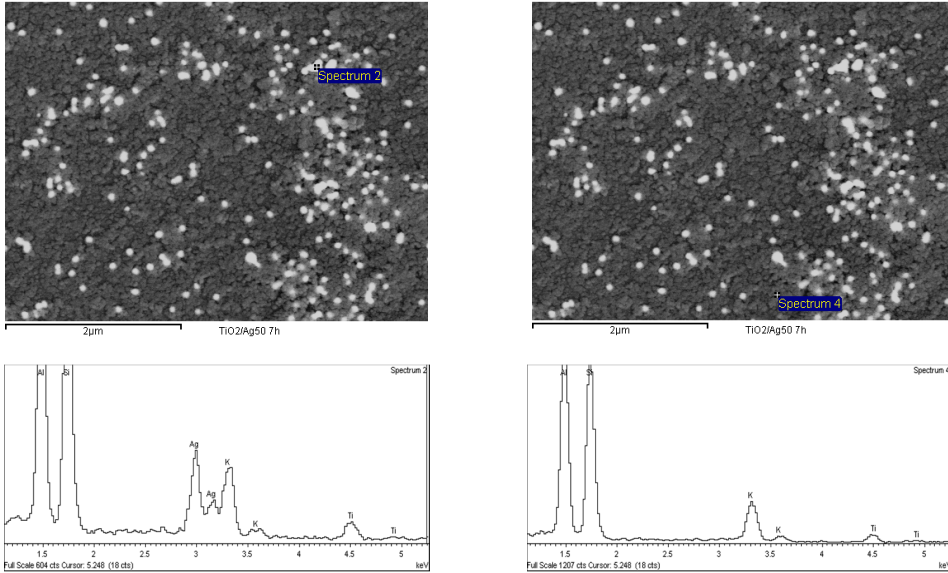Fig. 8. The EDS analysis of titanium dioxide/silver nanoparticle bilayers on mica (titanium dioxide nanoparticle coverage $\theta_{TiO2} = 0.40$, silver nanoparticle coverage $\theta_{Ag} = 0.01$).

As can be noticed, the experimental results shown in Fig. 9 remain in an agreement with the theoretical calculations (the solid lines) obtained from the random sequential adsorption model (RSA), described details in our previous works [17, 18]. In this model it is considered that the increase of silver nanoparticle coverage with the ionic strength is caused by the decrease in the range of the repulsive lateral interaction among adsorbed nanoparticles. Therefore, our studies demonstrate that the self-assembly process of titanium dioxide and silver nanoparticles carried out under given conditions of pH, ionic strength, will be useful for the preparation of bilayers of controlled coverage. It is also worth mentioning that such high coverage of silver nanoparticles deposited on titanium dioxide layers have not been described previously in the literature. For comparison, the most popular method of TiO_2/Ag preparation, which is based on the photochemical reduction of silver ions deposited on titanium dioxide coatings, allows to obtain silver nanoparticle coverage in the range from 0.003 to 0.04 [5].
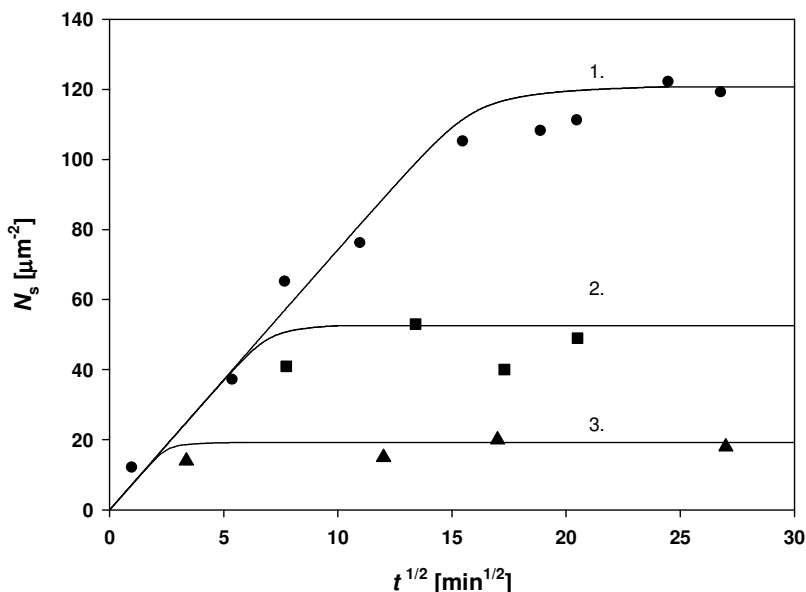
Fig. 9. The kinetics of silver nanoparticle adsorption on titanium dioxide monolayers deposited on mica surface, determined for ionic strength: 1. (●) 10^{-2} M NaCl, 2. (■) 10^{-3} M NaCl and 3. (▲) 10^{-4} M NaCl. The deposition conditions: pH 4.0, $T = 298$ K and the concentration of silver suspension 200 mg/dm^3. The points denote experimental data and the lines denote the theoretical results calculated from the random sequential adsorption model (RSA).

4. CONCLUSIONS

It was revealed that self-assembly processes are useful for the preparation of titanium dioxide/ silver nanoparticle bilayers on solid surfaces. It was shown that the efficient and reproducible preparation of such bilayers requires a careful determination of physicochemical properties of nanoparticle suspensions. For this reason, the range of nanoparticle stability and their electrokinetic properties were well-defined in for a broad range of ionic strength and pH. The formation of TiO_2/Ag bilayers was carried out at pH 4.0 for three selected ionic strengths. Systematic studies of silver nanoparticle deposition on titanium dioxide supporting layers, conducted by AFM and SEM imaging, confirmed that this process was diffusion controlled. Additionally, it was demonstrated that the coverage of external layer, governing average spacing among deposited nanoparticles can be regulated within broad limits by adjusting

the ionic strength of suspension as well as the deposition time. The deposition kinetics runs were adequately reflected for the entire range of times and ionic strength by the random sequential adsorption (RSA) model.

5. ACKNOWLEDGMENTS

REFERENCES

[1] Y.Q. Liang, Z.D. Cui, S.L. Zhu, Y. Liu, X.J. Yang, *J. Catal.*, **278**, 276, (2011).
http://dx.doi.org/10.1016/j.jcat.2010.12.011

[2] E. Grabowska, A. Zaleska, S. Sorgues, M. Kunst, A. Etcheberry, C. Colbeau-Justin, H. Remita, *J. Phys. Chem. C*, **117**, 1955, (2013).
http://dx.doi.org/10.1021/jp3112183

[3] Y. Yang, L. Qu, L. Dai, TS. Kang, M. Durstock, *Adv. Mater.*, **19**, 1239, (2007).
http://dx.doi.org/10.1002/adma.200602181

[4] Z. Starowicz, M. Lipińska, R.P. Socha, K. Berent, G. Kulesza, P. Ozga, *J. Sol-Gel Sci. Technol,***73**, 563, (2015).
http://dx.doi.org/10.1007/s10971-014-3522-2

[5] Z. Starowicz, M. Lipiński, K. Berent, R.P. Socha, K. Szczepano-wicz, T. Kruk, *Plasmonics*, **8**, 41 (2013).
http://dx.doi.org/10.1007/s11468-012-9412-y

[6] D. Wodka, E. Bielańska, R.P. Socha, M. Elżbieciak-Wodka, J. Gurgul, P. Nowak, P. Warszyński, I. Kumakiri, *Appl. Mater. Interfaces*, **2**, 1945 (2010).
http://dx.doi.org/10.1021/am1002684

[7] V. Ilie, D. Tomova, L. Bilyarska, A. Eliyas, L. Petrov, *Appl. Cata. B*, **63**, 266 (2006).
http://dx.doi.org/10.1016/j.apcatb.2005.10.014

[8] M.K. Seery, R. George, P. Floris, S. C. Pillai, *J. Photochem. Photobiol. A Chemistry,* **189**, 259 (2007).
http://dx.doi.org/10.1016/j.jphotochem.2007.02.010

[9]   F.B. Li, X.Z. Li, *Chemosphere*, **48**, 1103 (2002).
      http://dx.doi.org/10.1016/S0045-6535(02)00201-1
[10] Y. Tian, T. Tatsuma, *J. Am. Chem. Soc.* **127**, 7632 (2005).
      http://dx.doi.org/10.1021/ja042192u
[11] S. Anandan, P. Sathish Kumar, N. Pugazhenthiran, J. Madhavan,
      P. Muruthamuthu, *Sol. Energ. Mat. Sol.* **92**, 929 (2008).
      http://dx.doi.org/10.1016/j.solmat.2008.02.020
[12] A. Orlov, D.A. Jefferson, N. Macleold, R.M. Lambert, *Catal. Lett.*
      92, 41 (2004).
      http://dx.doi.org/10.1023/B:CATL.0000011084.43007.80
[13] K.H. Wang, Y.H. Hsieh, P.W. Chao, C.T. Chang, *J. Hazard.
      Mater.* **95**, 161 (2002).
      http://dx.doi.org/10.1016/S0304-3894(02)00135-8
[14] T. Sano, S. Kutsuna, N. Negishi, K. Takeuchi, *J. Mol. Catal/
      A: Chem.* **189**, 263 (2002).
      http://dx.doi.org/10.1016/S1381-1169(02)00353-9
[15] V. Iliev, D. Tomova, L. Bilyarska, L. Petrov, *Catal. Commun.* **5**,
      759 (2004).
      http://dx.doi.org/10.1016/j.catcom.2004.09.005
[16] X. Hou, M. Huang, X. Wu, A. Liu, *Chem. Eng. J.* **146**, 42 (2009).
      http://dx.doi.org/10.1016/j.cej.2008.05.041
[17] M. Oćwieja, Z. Adamczyk, M. Morga, A. Michna, *J. Colloid
      Interface Sci.*, **364**, 39, (2011).
      http://dx.doi.org/10.1016/j.jcis.2011.07.059
[18] M. Oćwieja, Z. Adamczyk, K. Kubiak, *J. Colloid Interface Sci.*,
      376, 1 (2012).
      http://dx.doi.org/10.1016/j.jcis.2012.02.017
[19] J.A. Creighton, Ch.G. Blatchford, M.G. Albrecht, *J. Chem. Soc.
      Faraday Trans.*, **75**, 790, (1979).
      http://dx.doi.org/10.1039/f29797500790
[20] P. Raveendran, J. Fu, S.L. Wallen, *J. Am. Chem. Soc.*, **125**, 13940
      (2003).
      http://dx.doi.org/10.1021/ja029267j
[21] Z. Li, Y. Wang, Q. Yu, *J. Mater. Eng. Perform.*, **19**, 252 (2010).
      http://dx.doi.org/10.1007/s11665-009-9486-7
[22] M. Oćwieja, Z. Adamczyk, *Surface Innovations,* **2**, 160 (2013).
      http://dx.doi.org/10.1680/si.13.00042

[23] M. Kujda. M. Oćwieja, Z. Adamczyk, O. Bocheńska, G. Braś, A. Kozik, E. Bielańska, J. Barbasz, *J. Nanosci. Nanotechnol.*, **15**, 3574, (2015).
http://dx.doi.org/10.1166/jnn.2015.9727

[24] X. Hong, Z. Wnag, W. Cai, F. Lu, J. Zhang, Y. Yang, Y. Liu, *Chem. Mater.*, **17**, 1548 (2005).
http://dx.doi.org/10.1021/cm047891k

[25] U. Kreibig, M. Vollmer, *Optical Properties of Metal Clusters*, Springer Series in Material Science, vol. 25, Springer, Berlin, Germany (1995).
http://dx.doi.org/10.1007/978-3-662-09109-8

[26] A.T. Vu, Q.T. Nguyen, T.H. L. Bui, M.C. Tran, T.P. Dang, T.K. H. Tran, *Adv. Nat. Sci.*, **1**, 015009 (2010).
http://dx.doi.org/10.1088/2043-6254/1/1/015009

[27] M. Kosmulski, *Surface charging and points of zero charge*, CRC Press, Boca Raton, FL 33487-2742 (2009).
http://dx.doi.org/10.1201/9781420051896

[28] P.J. Scales, F. Grieser, T.W. Healy, *Langmuir*, **6**, 582 (1990).
http://dx.doi.org/10.1021/la00093a012

[29] M. Oćwieja, Z. Adamczyk, M. Morga, E. Bielańska, A. Węgrzyno-wicz, *J. Colloid Interface Sci.*, **386**, 51 (2012).
http://dx.doi.org/10.1016/j.jcis.2012.06.056